

On common-offset prestack time migration with curvelets

Huub Douma* and Maarten V. de Hoop, Colorado School of Mines

Summary

Recently, curvelets have been introduced in the field of applied harmonic analysis and shown to optimally sparsify smooth (C_2 , i.e., twice continuously differentiable) functions away from singularities along smooth curves. In addition, it was shown that the curvelet representation of wave propagators is sparse. Since the wavefronts in seismic data lie mainly along smooth surfaces (or curves in two dimensions), and since the imaging operator belongs to the class of operators that is sparsified by curvelets, curvelets are plausible candidates for simultaneous sparse representation of both the seismic data and the imaging operator. In this paper, we mention the use of curvelets in wave-equation based imaging and we study the use of curvelets in common-offset (CO) pre-stack time migration. We focus on time migration as a preparation for wave-equation based imaging in heterogeneous media. We show that simply translating, rotating and dilating curvelets according to the CO pre-stack map time-migration equations, combined with amplitude scaling, provides a reasonable approximation to time-migration. We demonstrate the principle in two dimensions but emphasize that extension to three dimensions is possible using 3D equivalents of curvelets.

Introduction

The local slopes of reflections in seismic data, measured at the surface, determine (together with the velocity of the medium at the surface) the directions in which we need to ‘look into the earth’ from the surface, to find the location and orientation of the reflector in the subsurface where the reflection occurred. Provided the medium does not allow different reflectors to have identical surface seismic measurements (locations, times *and* slopes) that persist in being identical under small perturbations of the reflectors (see Douma & de Hoop (2005) for an explanation of this condition), the slopes at the source and receiver locations together with their respective locations and the reflection times can be mapped one-to-one to the reflector location *and* orientation in the image. This process is usually referred to as map migration [e.g., Douma & de Hoop (2005)]. In most seismic applications that make explicit use of the slopes (such as parsimonious migration, controlled directional reception, and stereo tomography) the slopes are estimated from the data using additional processing techniques such as local slant-stacking or multidimensional prediction-error filters.

In the field of applied harmonic analysis, curvelets were recently introduced (Candès & Donoho., 2000; Candès & Guo, 2002; Candès & Donoho, 2004) and shown to provide an essentially optimal representation of objects that are twice continuously differentiable (C^2) away from discontinuities along C^2 edges. Due to the wave character of seismic data, the reflections recorded in seismic data lie mainly along smooth surfaces (or curves in 2D), just as geologic interfaces in the subsurface lie primarily along smooth surfaces. Therefore, it is plausible to assume that seismic data and their images can be sparsely represented using curvelets. This was earlier also noted by Herrmann

(2003). Since curvelets are anisotropic 2D extensions of wavelets and have a direction associated with them, using curvelets as building blocks of seismic data, the slopes in the data are built into the representation of the data; a simple projection of the data onto the curvelet frame (combined with an intelligent thresholding scheme to separate signal from noise) then gives the directions associated with the recorded wavefronts.

Smith (1998) and later Candès and Demanet (2002) have shown that curvelets sparsify a certain class of Fourier integral operators. Since the seismic imaging operator can be constructed from Fourier integral operators that belong to this class, and since reflections in seismic data lie mainly along smooth curves, it seems that curvelets are plausible candidates for simultaneous compression of seismic data and the imaging operator. Curvelets have a multiresolution character just like wavelets do. Hence curvelets of different scales have different dominant wavelengths. It is known that waves with a certain dominant wavelength are sensitive to variations in the medium with certain length scales only; i.e., a wave with a dominant wavelength of say 100 meters is hardly sensitive to variations in the medium on the scale of one centimeter. Therefore curvelets of different scales are sensitive to media with variations on different scales. This allows the possibility to filter the background velocity with filters related to the dominant wavelength of the curvelets (i.e., the scale of the curvelets), and propagate curvelets of different scales through different media. Smith (1998) has shown that the propagation of a curvelet through such filtered media is governed by the Hamiltonian flow associated with the center of the curvelet. Here the center of the curvelet is its center in phase-space, meaning the center location of the curvelet combined with the center direction. This means that a curvelet is treated as if it was a particle with an associated momentum (or direction). For each filtered medium, this observation reduces to the statement of Candès and Demanet (2004) that the propagation of a curvelet (through an infinitely smooth medium) is “well-approximated by simply translating the center of the curvelet along the corresponding Hamiltonian flow.” This implies that curvelets remain fairly localized in both the spatial domain and the spectral domain. In fact, the procedure just outlined yields a leading order contribution to the solution of the wave equation (Smith, 1998). Hence this procedure admits wave-equation-based seismic imaging with curvelets. For CO time migration, Douma & de Hoop (2004) showed that indeed a curvelet remains fairly localized in both the spatial and spectral domain after such migration.

For homogeneous media the above mentioned filtering is unnecessary. For such media, wave-equation based seismic imaging is really the same as Kirchoff-style imaging. Here, we study the use of curvelets in homogeneous media (i.e., in time migration) and verify the statement that curvelets can be treated as particles with associated directions (or momenta) in an imaging context. We focus on the simple case of homogeneous media in an attempt to learn the basic characteristics of seismic imaging with curvelets, as a preparation for imaging in heterogeneous media with curvelets. This work is a follow-up on earlier work (Douma & de Hoop, 2004) that showed that (at least

On common-offset prestack time migration with curvelets

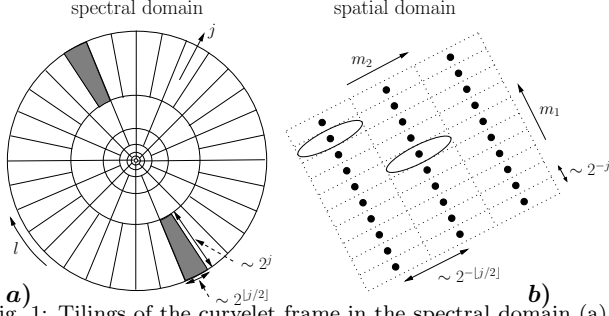


Fig. 1: Tilings of the curvelet frame in the spectral domain (a) and the spatial domain (b). The essential support of a curvelet in the spatial domain is indicated by an ellipse.

for time-migration) the kinematics of seismic imaging with curvelets are governed by map migration.

Curvelets

Curvelets are anisotropic 2D extensions of wavelets that have a direction associated with them. Just like wavelets are ‘localized’ in one variable and its Fourier dual, curvelets are ‘localized’ in two variables and their two Fourier duals. The spectral domain is subdivided into dyadic annuli (or subbands) which are subsequently divided into angular wedges (Figure 1a). Each wedge is indexed uniquely by a scale index j that determines the annulus, and an angular index l which determines the particular wedge within an annulus. The number of wedges in an annulus with scale j doubles every other annulus (or scale). The length (radial direction) equals the width (angular direction) squared (Figure 1a). This is generally referred to as *parabolic scaling*. To obtain a tiling of the spatial domain, each wedge is multiplied by a 2D orthonormal Fourier basis that just covers this wedge and which has the same orientation as this wedge (Figure 1b); in this way the sparsest sampling of the spatial domain is obtained. As a consequence the orientation of the tiling of space is different for each particular wedge in an annulus (Figure 1b). The location on the spatial lattice is determined by two translation indices m_1 and m_2 . Hence a curvelet is uniquely determined by the multi-index $\mu = (j, l, m_1, m_2)$. Intuitively, curvelets can be thought of as small pieces of bandlimited plane waves; the difference between this rough description and the actual interpretation being that a bandlimited plane wave has associated with it only one \mathbf{k} -direction, while a curvelet is associated with a small range of \mathbf{k} vectors. Curvelets form a tight frame for $L^2(\mathbb{R}^2)$, which can roughly be thought of as a basis with nonorthogonal basis elements.

Even though the curvelets used in this paper are 2D, they can be extended to higher dimensions. Figure 2 shows an example of a 3D curvelet in both the spatial domain (a) and the spectral domain (b). In the spatial domain, 3D equivalents of curvelets are roughly smoothed circular pieces of a bandlimited plane wave in $3D^1$.

CO time migration with curvelets

Using curvelets as building blocks of seismic data, the

¹This rough description of course ignores that each curvelet has a small range of \mathbf{k} -directions associated with it, rather than only a single \mathbf{k} direction, as has a plane wave.

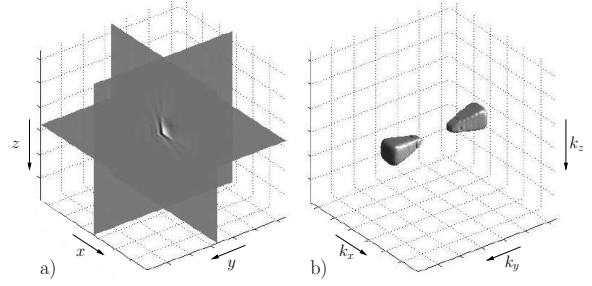


Fig. 2: A 3D equivalent of a curvelet in the spatial domain (a) and a contour plot of its associated spectrum (b).

directions (or local slopes) in the data follow from a straightforward projection of the data onto the curvelet frame. Thresholding of the curvelet coefficients then gives the curvelets associated with the main wavefronts in the data, and thus the directions associated with these wavefronts also. Subsequently, these directions can be used in the CO map time-migration equations from Douma & de Hoop (2005, their equations (7), (8), and (11) restricted to 2D) to determine the migrated location and orientation of the curvelet after migration. Hence, these equations determine a translation and a rotation of a curvelet.

It is known (e.g., Bleistein *et al.* (2000), p.223 and p.235) that after pre-stack migration, the length of the \mathbf{k} -vector changes according to

$$|\mathbf{k}| = \omega \nabla_{\mathbf{y}} \phi(\mathbf{y}, \mathbf{x}_s, \mathbf{x}_r) = \frac{\omega}{v(\mathbf{y})} \cos \theta(\mathbf{y}, \mathbf{x}_s, \mathbf{x}_r), \quad (1)$$

where ω is the angular frequency, $\mathbf{x}_{s,r}$ are the source and receiver locations, \mathbf{y} is the output location in the image, $\phi(\mathbf{y}, \mathbf{x}_s, \mathbf{x}_r)$ is the two-way traveltime from the source location \mathbf{x}_s to the reflector at \mathbf{y} to the receiver position \mathbf{x}_r , $v(\mathbf{y})$ is the velocity at output location \mathbf{y} , and $\theta(\mathbf{y}, \mathbf{x}_s, \mathbf{x}_r)$ is the half opening-angle between the ray from the source to the scattering point and the ray from the receiver to the scattering point. The term $\cos \theta(\mathbf{y}, \mathbf{x}_s, \mathbf{x}_r)$ is usually referred to as the *obliquity* factor. In 2D, for a constant background velocity and a CO acquisition geometry, equation (1) simplifies to $|\mathbf{k}| = \omega \cos \theta(x_m, t_m, x_u, h)/v$, where h is the half offset, x_u the common midpoint location along the 2D acquisition profile, x_m and t_m are the migrated horizontal location and migrated two-way traveltime, and the angle $\theta(x_m, t_m, x_u, h)$ is given by

$$\theta(x_m, t_m, x_u, h) = \frac{1}{2} \left\{ \tan^{-1} \left(\frac{2(x_u + h - x_m)}{vt_m} \right) - \tan^{-1} \left(\frac{2(x_u - h - x_m)}{vt_m} \right) \right\}. \quad (2)$$

A curvelet has dominant wavelength λ_c in the direction orthogonal to the curvelet (see Figure 3). However, the dominant wavelength λ in the vertical direction determines the frequency relevant to migration. It follows that $\lambda_c = \lambda \cos \theta_u$, which gives

$$\omega = \omega_c \cos \theta_u, \quad (3)$$

where θ_u is the phase-angle (measured clockwise positive with the vertical) of the curvelet in the data domain. Combining equations (1) and (3) it follows that, after migration,

On common-offset prestack time migration with curvelets

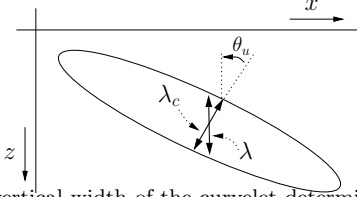


Fig. 3: The vertical width of the curvelet determines the wavelength λ relevant to seismic migration.

the length of the \mathbf{k} -vector can be written as

$$|\mathbf{k}| = \frac{\omega_c}{v(\mathbf{y})} \cos \theta(x_m, t_m, x_u, h) \sqrt{1 - (v(\mathbf{y})p_u)^2}, \quad (4)$$

where we used $\cos \theta_u = \sqrt{1 - (v(\mathbf{y})p_u)^2}$, with p_u the horizontal slowness in an unmigrated CO section. This means that the curvelet needs to be dilated (or stretched) in the image domain with dilation factor D given by

$$D = \frac{1}{\cos \theta(x_m, t_m, x_u, h) \sqrt{1 - (vp_u)^2}}. \quad (5)$$

where we specialized to the constant background velocity case. Therefore, CO pre-stack time migration with curvelets can be done by translating and rotating the curvelets in the data domain according to the map migration equations, and dilating the curvelets with a stretch factor given by equation (5). Throughout this paper, we refer to this transformation as the *TRD transformation*.

The TRD transformation of a curvelet provides the kinematics of imaging with curvelets, but ignores the dynamics, often referred to as the ‘true amplitude’ part of seismic imaging. For the purpose of this paper we simply scale the curvelet with

$$A(\mathbf{y}, x_u; h) = \frac{4y_3 \sqrt{r_s + r_g} (r_s^2 + r_g^2) \cos \theta(\mathbf{y}, x_u, h)}{(v r_s r_g)^{3/2}}, \quad (6)$$

where $r_{s,g}$ are the distance from the output location \mathbf{y} to the source and receiver at $x_s = (x_u - h, 0)$ and $x_r = (x_u + h, 0)$. This amplitude is part of the kernel of the 2.5-D CO Kirchhoff time migration [see equation (6.3.25) from Bleistein *et al.* (2000)], but ignores the frequency dependence of the amplitudes. To find the proper frequency dependence for the migration of a curvelet, we would really need to use a curvelet as scattered data u_S and evaluate the integrals in equation (6.3.25) from Bleistein *et al.* (2000) using a stationary phase analysis. At the moment of writing this paper, we have not done such an analysis. For the purpose of generating the results in this paper, we simply scale the curvelet with $A(\mathbf{y}, x_u; h)$ and restrict ourselves to migrating curvelets with the same frequency content (i.e., the same scale) only, to avoid the issue of proper weighting with frequency.

Numerical examples

Figure 4a shows a 2.5-D CO Kirchhoff migrated curvelet, while Figure 4d shows the real part of the associated spectrum. Figure 4b shows the result of the TRD transformation of the same curvelet, while Figure 4c shows the difference between the Kirchhoff migrated curvelet and the TRD transformed curvelet. Before subtraction, both

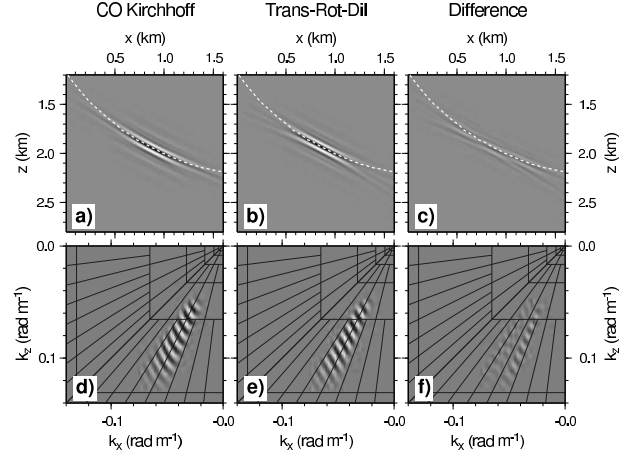


Fig. 4: 2.5-D CO Kirchhoff migration of a curvelet (a), TRD transformation of a curvelet combined with amplitude scaling (b), and their difference (c). The real part of the spectra associated with Figures a, b, and c, are shown in d, e, and f, respectively. The dashed white line shows part of the associated isochron.

images were normalized to have maximum amplitude one, such that the difference only shows relative amplitude differences between both images. Figures 4e and f show the real part of the amplitude spectra of the images shown in Figures 4b and c. It is clear that for this particular curvelet, the TRD transformation of the curvelet gives a reasonable approximation to the Kirchhoff result. The maximum amplitude of the difference between both methods is about 20% of the maximum amplitude in the Kirchhoff image. From the real part of the spectrum we see that the curvelet is slightly bent due to the migration, whereas the TRD transformation does not take this bending into account (cf. Figures 4d and e). The main difference in the spectrum occurs on the edges of the support of the curvelet in the frequency domain, where this bending is strongest.

Figure 5a shows a superposition of 8 curvelets, with the same central location in space, and the same scale index, but different directions (or angular indices). The vertical axis is here again converted from two-way traveltime to depth. Figure 5b shows the amplitude spectrum of all 8 curvelets combined, and it is clear that we used curvelets that have leftward pointing \mathbf{k} -vectors only. Figure 5c shows the 2.5-D CO Kirchhoff migrated result, while Figure 5d shows the result of our TRD transformation combined with an amplitude scaling given by equation (6). Note how the Kirchhoff result gives the left part of the isochron only. Comparing Figures 5c and d, the TRD transformation combined with the amplitude correction of equation (6) gives a reasonable approximation to the Kirchhoff migrated result. The interference of the different curvelets (of the same scale) is good, and compares favorably to the Kirchhoff result, although the comparison seems better for the shallower dipping part of the isochron. At the steeper parts of the isochron, the destructive interference between different curvelets away from the isochron, is somewhat less effective and leaves the tails of the curvelets somewhat visible.

In order to see the differences between the results for the steeper dipping curvelets and the shallower ones, Figure 6 shows the comparison between the Kirchhoff result and our TRD transformation for both a shallow and a steeply dip-

On common-offset prestack time migration with curvelets

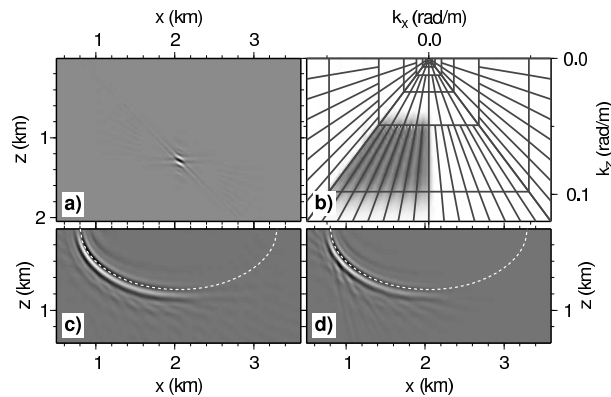


Fig. 5: Superposition of 8 curvelets (a), the associated spectrum (b), the 2.5-D CO Kirchhoff migrated result (c), and the result from the TRD transform with amplitude correction (d).

ping curvelet. Here we did zero-offset migration, to avoid the curvature of the isochron being different at different locations on the isochron. Figure 6 shows that the steeper dipping curvelet is significantly ‘bent’ towards the isochron, while the shallower dipping curvelet is hardly bent at all. As a result, the TRD transform does better for the shallower dipping curvelets than for the steeper dipping ones, as it does not include any such bending. It remains to be seen how severe the error is if we ignore this bending, and use our TRD transform on a synthetic data-set with many curvelets. In this case, there would be interaction between curvelets from several different scales, i.e., with different frequency content. Such a test would require the proper frequency weighting for curvelets of different scales.

We calculate the TRD transform using a brute-force approach in the spatial domain; for the significant curvelet coefficients, we apply an inverse curvelet transform, and transform the resulting curvelet in the spatial domain according to our TRD transform. This approach allows us to show the proof of concept of imaging with curvelets using our TRD transform, but does not provide an efficient way to do such imaging with curvelets. Ultimately one would want to calculate the TRD transform in the curvelet frame through a mapping of curvelet coefficients.

Conclusion

We have presented first examples of the use of curvelets in CO pre-stack time migration. Since curvelets are roughly like pieces of bandlimited plane waves, the wave-character of the seismic data can be built into the representation of the data. Therefore, in essence, curvelets are an appropriate reparameterization of seismic data. The numerical tests of 2D CO pre-stack time imaging with curvelets we presented, showed that our simple TRD transformation of curvelets provides a reasonably accurate approximation to the Kirchhoff migrated result, at least on a per scale basis. Our results for CO pre-stack time migration with curvelets in 2D can be extended to 3D using 3D equivalents of curvelets.

Acknowledgments

We thank Emmanuel Candès for providing us with his Matlab implementation of the digital curvelet transform via unequally spaced fast Fourier transforms. This work was partly supported by Total E & P and the sponsors of

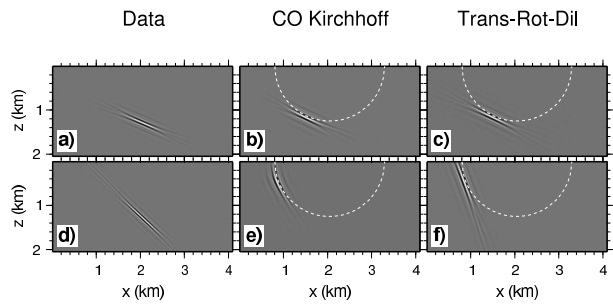


Fig. 6: A shallow dipping curvelet (a) and a steeply dipping curvelet (d), their zero-offset Kirchhoff migrated counterparts (b and e) and the TRD transformed counterparts (c and f).

the Consortium Project on Seismic Inverse Methods for Complex Structures at the Center for Wave Phenomena.

References

- Bleistein, N., Cohen, J., and Stockwell, J., 2000, Mathematics of multidimensional seismic imaging, migration, and inversion, Springer.
- Candès, E. J., and Demanet, L., 2004, The curvelet representation of wave propagators is optimally sparse: submitted, and can be downloaded from Candès website.
- Candès, E., and Donoho, D., 2000, Curvelets - a surprisingly effective nonadaptive representation for objects with edges, in Rabut, C., Cohen, A., and Schumaker, L., Eds., Curves and Surfaces: Vanderbilt University Press, 105–120.
- Candès, E. J., and Donoho, D. L., 2004, New tight frames of curvelets and optimal representations of objects with piecewise C^2 singularities: Comm. on Pure and Appl. Math., **57**, 219–266.
- Candès, E. J., and Guo, F., 2002, New multiscale transforms, minimum total variation synthesis: Applications to edge-preserving image reconstruction: Signal Processing, **82**, 1519–1543.
- Douma, H., and de Hoop, M., 2004, Wave-character preserving pre-stack map migration using curvelets: Expanded Abstracts 74th annual international meeting of the SEG.
- Douma, H., and de Hoop, M. V., 2005, Explicit expressions for pre-stack map time-migration in isotropic and VTI media and the applicability of map depth-migration in heterogeneous anisotropic media: *Accepted for publication in Geophysics*.
- Herrmann, F. J., 2003, Multifractional splines: application to seismic imaging, in Michael A. Unser Akram Aldroubi, A. F. L. E., Ed., Proceedings of SPIE Technical Conference on Wavelets: Applications in Signal and Image Processing X, Volume 5207: SPIE, 240–258.
- Smith, H., 1998, A parametrix construction for wave equations with $C^{1,1}$ coefficients: Ann. Inst. Fourier, **48**, 797–835.